



## Enhancement of Electrical and Magnetic Properties of Nanocomposite BaTiO<sub>3</sub> - NiZnFe<sub>2</sub>O<sub>4</sub> Irradiated by Gamma Ray

A.M.A. Henaish <sup>\*1</sup>, A.H. Ashour<sup>2</sup>, D.E. El Refaay<sup>3,4</sup> and O.M. Hemedat<sup>1</sup>

1. Physics Department, Faculty of Science, Tanta University, Egypt

2. Radiation Physics Department, National Center for Radiation Research and Technology, Atomic Energy Authority, Egypt

3. Physics Department, Faculty of Science, Suez Canal University, Egypt

4. King Khalid University, College of Science and Arts, SUA

Received 8<sup>th</sup> May 2018

Accepted 19<sup>th</sup> Feb. 2019

The effects of gamma ray irradiation on the, microstructural and magnetic properties of the composite (1-x) (Ni<sub>0.8</sub>Zn<sub>0.2</sub>Fe<sub>2</sub>O<sub>4</sub>) + x (BaTiO<sub>3</sub>) where x = 0%, 20%, 40%, 60% and 80% BT content have been investigated. All samples were exposed to 310 kGy gamma radiation dose at a dose rate of 1.4 kGy/h at room temperature using <sup>60</sup>Co radioactive source at irradiation cell (medical sterilizer type CM-20). From X-ray diffraction analysis, it was found obviously that the lattice parameters and the average grain size have been affected, for all irradiated samples. The initial permeability at Curie temperature for all samples sharply decreased after irradiation. The values of diffusion coefficient of oxygen vacancies, the concentration of oxygen vacancies and the activation energy of diffusion process were calculated before and after irradiation. From the results, it could be concluded that the material after irradiation can be used for the Gamma ray detection.

**Keywords:** Nickel–zinc ferrites, BaTiO<sub>3</sub>, Nanocomposites, Gamma ray irradiation

### Introduction

Recently, composites especially ferromagnetic-ferroelectric phases, have been attracting more attention [1]. Composites (which possess two or more types of orders simultaneously) are considered to be promising materials for applications such as, electrically controlled microwave phase shifters or ferromagnetic resonance devices, magnetically controlled electro-optics or piezoelectric devices, broadband magnetic field sensors, and (ME) memory devices. The technological application of magnetic permeability is very important in Magnetic Temperature Transducers (MTT) devices and for magnetic switches. Studying the magnetic permeability as a function of temperature before and after irradiation with  $\gamma$ -ray is of utmost

importance to define the effect of radiation exposure.

When ferromagnetic and ferroelectric phases (piezoelectric/piezomagnetic composite materials) coexist in one material, they exhibit magneto-electric effect (ME) [2 - 4]. The (ME) phenomena occurs due to the interaction between magnetization and electric polarization. The (ME) is due to the mechanical coupling between ferrite and ferroelectric phases.

The aim of the present study is to improve the electrical and magnetic properties of the nanocomposites after gamma radiation.

### Experimental Producers

*Synthesis of BaTiO<sub>3</sub> and NiZnFe<sub>2</sub>O<sub>4</sub> composite samples*

The composite samples of BaTiO<sub>3</sub> and NiZnFe<sub>2</sub>O<sub>4</sub> were prepared using a conventional double sintering ceramic process. The BaTiO<sub>3</sub> was prepared starting from BaCO<sub>3</sub> and TiO<sub>2</sub> powders. The powder mixture was ground for 10 hrs then presintered at 1000°C for 16 hrs. Similarly, Ni<sub>0.8</sub>Zn<sub>0.2</sub>Fe<sub>2</sub>O<sub>4</sub> compound was prepared from NiO, ZnO and Fe<sub>2</sub>O<sub>3</sub> oxides powders of 99.99% purity. The oxides were mixed in stoichiometric ratio for 10 hrs then presintered at 950 °C for 16 hrs and left to be cooled gradually to reach room temperature. Then, the two phases were mixed and ground very well for 12 hrs using agate mortar to form BT+NZF. After that, pellets using different stainless steel molds were formed under a pressure of 10 ton/cm<sup>2</sup>: (1) tablet of diameter 1 cm and 0.4 cm thickness; and (2) toroid of external diameter 3 cm, internal diameter 2 cm and height 0.5 cm. Finally, the samples were sintered at 1200 °C for 8 hrs. The furnace was left to cool down a room temperature with a constant rate of 2.5 °C/min.

#### *γ-Rays irradiation*

All investigated samples were irradiated using γ-rays of <sup>60</sup>Co radioactive source at room temperature using irradiation cell (medical sterilizer type CM-20) in the cyclotron facility, Nuclear Research Center, Atomic Energy Authority, Cairo, Egypt. The total exposure dose was 310 kGy with dose rate 1.4 kGy/h. The irradiated samples were measured using the abovementioned techniques to study the effect of γ irradiation on their properties.

#### *Characterizations*

The phase composition of the prepared composite after irradiation was analyzed using XRD diffractometer of type (D8 Advance, Bruker AXS, 40 KV, 40 mA) with monochromatic Cu-Kα (λ = 1.54960 Å). The morphology of the samples was identified using the scanning electron microscope (SEM) (JOEL, Model: JSM-5600, Japan.). An RLC bridge type BM-591 was used for the measurement of DC resistivity and permeability for the prepared BT+NZF composite at 1 KHz. More details about the system are reported in a previous study [5]. The DC electrical resistivity

measurements were performed after coating the samples uniformly with silver paste.

DC resistance was measured using an Electrometer (Keithely 610 C). The activation energy of charge carriers was calculated from the relation [6]

$$\rho = \rho_0 e^{\frac{-E}{KT}}$$
, where ρ<sub>0</sub>: is pre-exponential constant, E is the activation energy in eV, which was calculated from the slop of ln ρ vs. (1000/T) K<sup>-1</sup>.

The magnetic permeability (μ<sub>i</sub>) of composite samples were measured using toroid at a constant frequency f= 1 KHz, in the temperature range from room temperature up to 825 K. The initial permeability (μ<sub>i</sub>) was estimated using the following formula [7]

$$\mu_i = \frac{L}{L_0}$$
, where L: is the inductance of the toroid in Henry.

$$L_0 = 2.6 N^2 d \log\left(\frac{A}{B}\right) * 10^{-9} H$$
, where

N: is the number of turns, d: thickness of toroid, A: is the outer diameter and B is the inner diameter.

## **Results and Discussion**

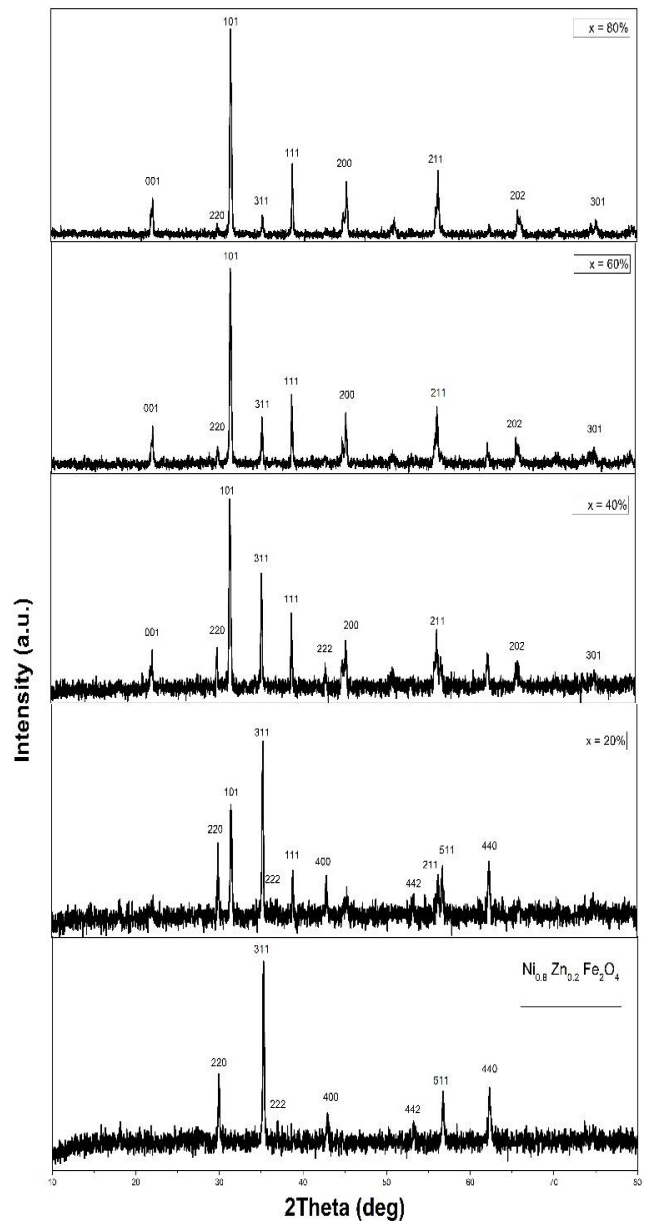
### *X-ray diffraction analysis*

The x-ray diffraction patterns for the pure NZF, BT and the composite BT+NZF are shown in Fig. (1a, 1b). before and after irradiation with γ-rays. The patterns confirmed the formation of pure single phase for both perovskite BT and ferrimagnetic phase NZF, with small shift in 100% diffraction peak. By increasing BT content, the intensity of 100% (311) decreases while the 100% (101) peak for BT increases. For composite samples the XRD patterns shows the existence of two piezoelectric and pizomagnetic phases. The lattice constant and the crystallite size were deduced from the analysis of XRD before and after irradiation with γ-rays. The lattice constant before irradiation of ferromagnetic phase did not change remarkably with the increase of the BT content, but slightly changed for tetragonal phase (the lattice constant (c) decrease whereas (a) increase).

The XRD patterns of the irradiated samples showed a slight shift of the reflected peaks and an increasing trend of crystallite size which is attributed to the induced defects and compressive strain of the crystal lattice. Some distortions occur in the lattice after  $\gamma$ -irradiation which is similar to what was reported in a previous work of Mn-Ni ferrite [8] and for Mg-Mn nano-ferrites [9, 10]. The lattice parameters ( $c$ ) decrease after irradiation which means that the tetragonality of the ferroelectric phase decrease. The results showed that the lattice parameters of NZF increase after irradiation for the sample with BT content (20, 40 and 80%). This can be attributed to the interaction of  $\gamma$ -rays with the outer electrons of the  $\text{Fe}^{3+}$  content in the lattice (radius  $0.64 \text{ \AA}$ ) enforcing it to convert to ferrous ions  $\text{Fe}^{2+}$  with large radius ( $0.76 \text{ \AA}$ ). The process of transformation of  $\text{Fe}^{3+}$  to  $\text{Fe}^{2+}$  was suggested through the following reaction:



The porosity was increased after irradiation due to the formation of defects and vacancies which leads to increase of porosity.



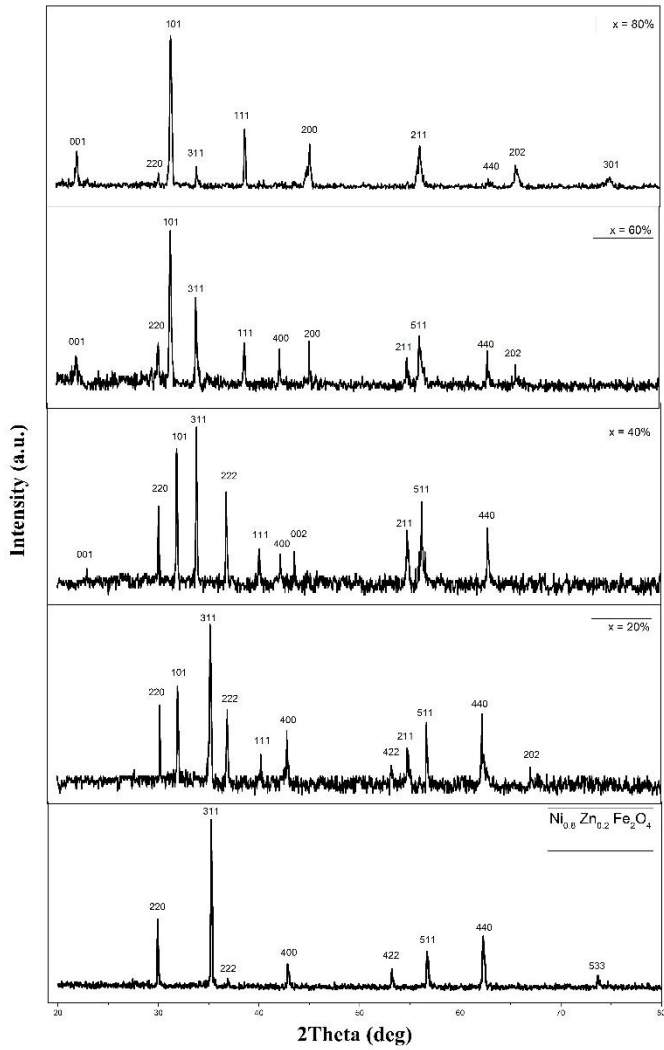


Fig. (1-a): X-ray diffraction patterns of composite (1-X)  $\text{Ni}_{0.8}\text{Zn}_{0.2}\text{Fe}_2\text{O}_4 + (x) \text{BaTiO}_3$  before irradiated with gamma ray

Fig. (1-b): X-ray diffraction patterns of composite (1-X)  $\text{Ni}_{0.8}\text{Zn}_{0.2}\text{Fe}_2\text{O}_4 + (x) \text{BaTiO}_3$  irradiated with gamma ray

The estimated crystallite size, lattice parameters, curie temperature, porosity and activation energy for the unirradiated and irradiated sample samples are given in Table (1).

Table (1): The measured values of crystallite size, lattice parameters, curie temperature, porosity and activation energy for the unirradiated (D0) and irradiated sample (D1) samples

Parameter	X=0		X=20		X=40		X=60		X=80	
	D <sub>o</sub>	D <sub>1</sub>								
Crystallite size, (nm)	30.688	45.365	22.586	43.462	24.90	47.463	23.968	24.297	27.240	31.238
Lattice parameters, a <sub>exp</sub>	8.429	8.512	8.422	8.433	8.507	8.440	8.513	8.421	8.512	8.670
Porosity	0.458	0.441	0.545	0.533	0.309	0.353	0.256	0.299	0.367	0.376
Curie temperature, T <sub>c</sub> (K) from DC measurements.	593	556	653	601	663	605	603	566	623	700
Activation energy, E <sub>f</sub> (eV)	0.643	0.373	0.593	0.386	0.530	0.338	0.682	0.302	0.674	0.277

### DC conductivity

Figure (2a) shows the D.C. resistivity as a function of reciprocal temperature  $1000/T$  at different BT content for the composite samples. It is known that all curves have three regions with two point breaks. Each region has its own conduction mechanism and activation energy, the second region represents the ferrimagnetic region and the second break point  $T_2$  represents the curie temperature at which the ferrimagnetic phase undergoes first order transition from ferrimagnetic to paramagnetic state. The conduction mechanism in this region is the hopping conduction mechanism where the charge is localized to the lattice and the conduction occurs by thermal activation of mobility of charge carriers [8].

The conductivity at low temperature (first region) belongs to the band theory conduction mechanism and the materials behave as semiconductors, where Ba ion acts as donor and some interaction occurs between Ti ions which depends on Ti-Ti distance. The values of the activation energy of the hopping conduction region ranged from (0.4-0.9 eV), suggesting the presence of polaron hopping conduction mechanism. The increase of activation energy which is corresponding to the increase of resistivity with increasing BT suppresses the hopping process and increases the distance between  $Fe^{3+}$  and  $Fe^{2+}$  leading to increase of activation energy and D.C. resistivity.

The D.C. resistivity after irradiation as a function of reciprocal temperature is shown in Fig. (2-b). From this figure, it was seen that the D.C. resistivity increases sharply for the samples (0, 20, 40 and 60 % BT content) and decreases for the latest sample 80 and 100% BT content. The irradiation process is associated with the decrease of  $T_c$  for sample (0, 20, 40 and 60 % BT content) and the increase for 80 and 100% BT content. This behavior can be explained using the results of x-rays analysis, where the tetragonality decreases after irradiation. The  $\gamma$ -ray destroyed the crystal cell and the crystal becomes non-symmetrical, which facilitate the transition from ferri to para state and it takes place at low temperature. This explains the decrease of Curie temperature  $T_c$  after irradiation. The higher value of BT content leads to increasing  $T_c$ , which is correlated by the increase of particle size of the samples after irradiation.

### *The diffusion coefficient*

The diffusion coefficient of oxygen vacancies for the composite samples  $Ni_{0.8}Zn_{0.2}Fe_2O_4+x$  ( $x$ )  $BaTiO_3$ , where ( $x=0, 20, 40, 60, 80$  %) before and after irradiation are shown in Figs. (3a, 3b) as a function of reciprocal temperature. It is illustrated from the figure that the diffusion coefficient increases with increasing temperature due to the increase of thermal activation mobility of oxygen vacancies .

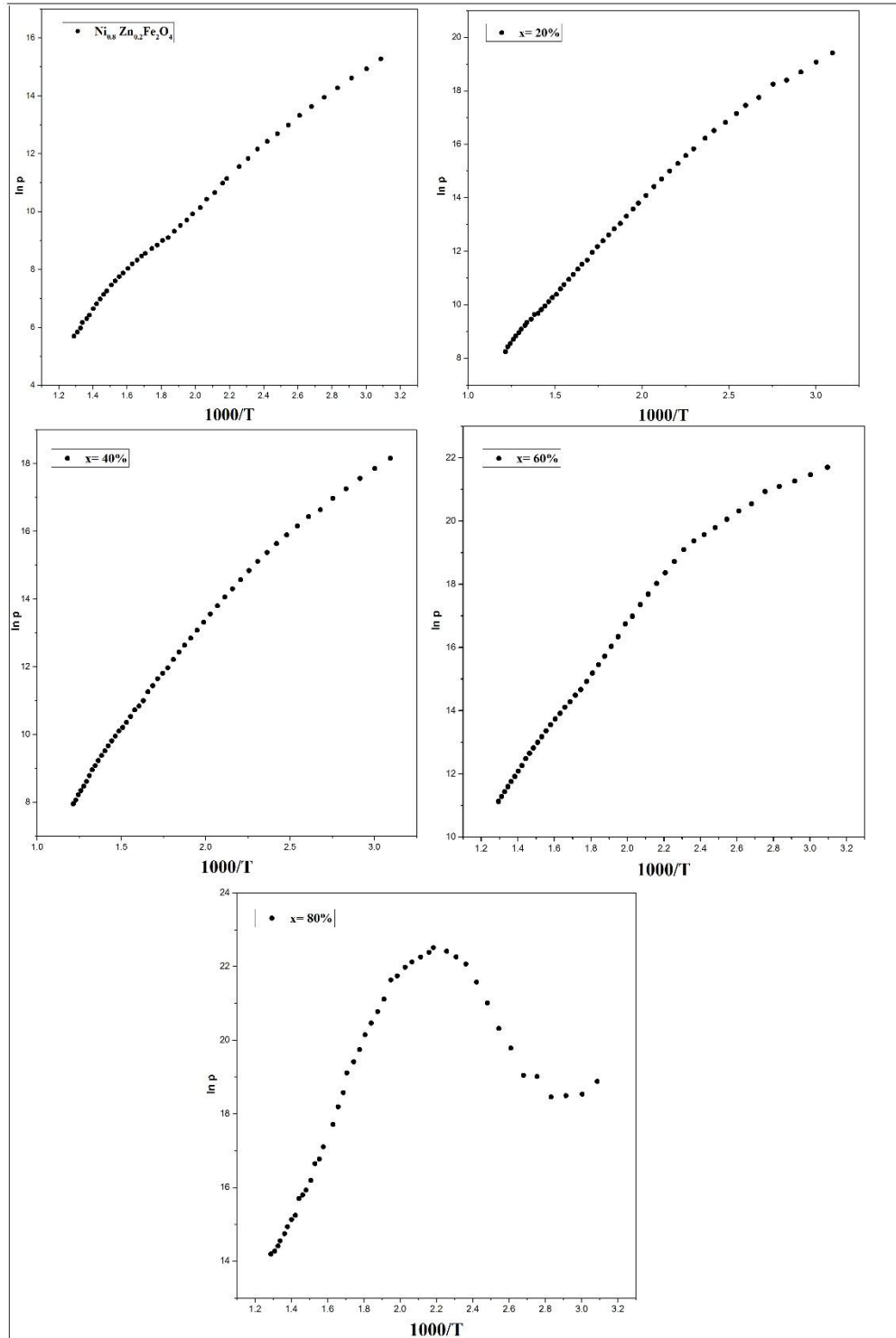


**Fig. (2-a):** Variation of DC conductivity of the composite  $(1-x)\text{Ni}_{0.8}\text{Zn}_{0.2}\text{Fe}_2\text{O}_4 + x\text{BaTiO}_3$  as a function of reciprocal temperature before irradiated with gamma ray

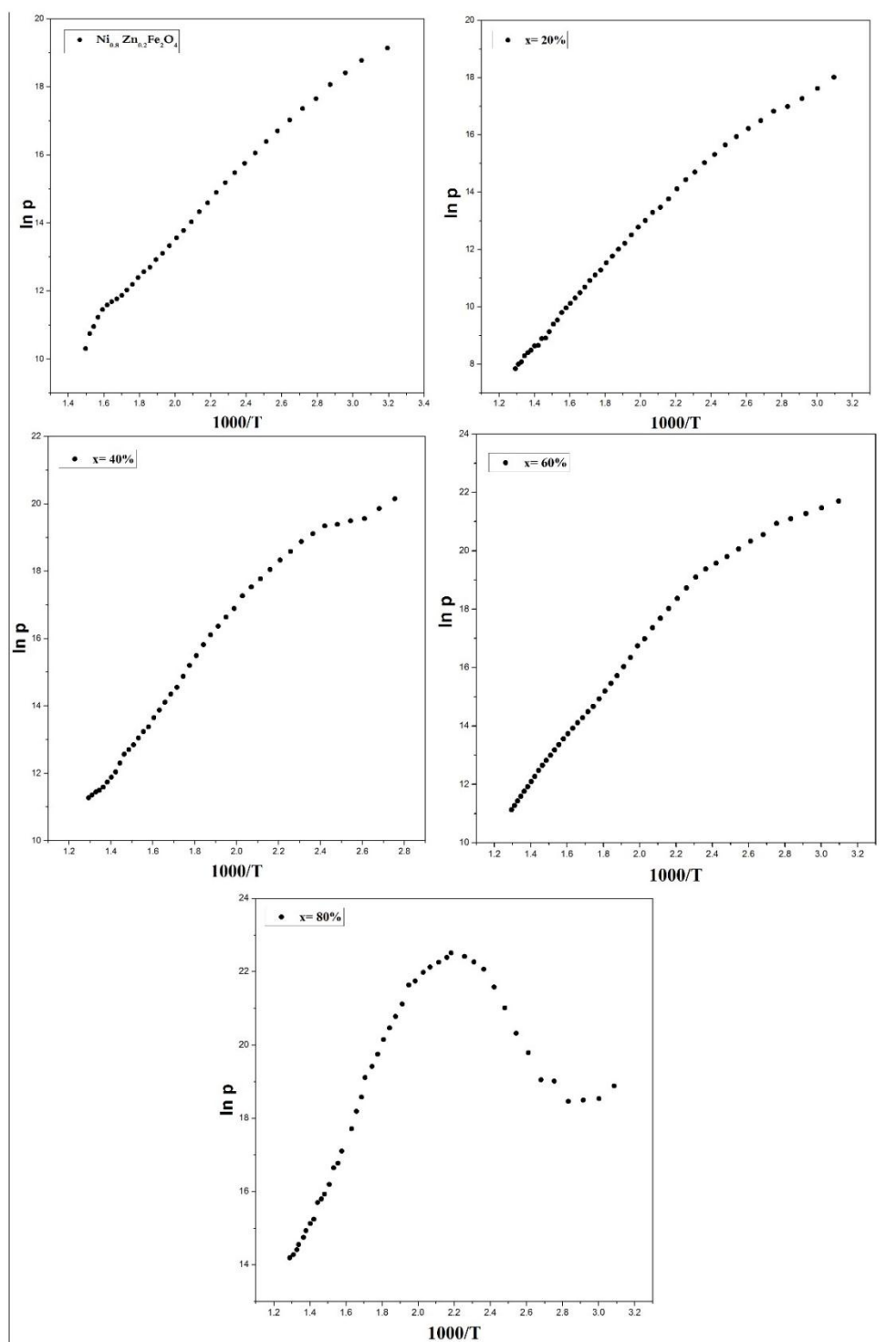


Fig. (2-b): Variation of DC conductivity of the composite  $(1-x)\text{Ni}_{0.8}\text{Zn}_{0.2}\text{Fe}_2\text{O}_4 + (x)\text{BaTiO}_3$  as a function of reciprocal temperature after irradiated with gamma ray

The diffusion coefficient ( $D$ ) of oxygen vacancies was estimated from the equation [11].

$$D = \frac{\sigma K_B T}{N e^2}$$

Where ( $\sigma$ ) is the DC electrical conductivity, ( $N$ ) the number of atoms/ $m^3$  equal to  $4 \cdot 10^{28} m^{-3}$ , ( $e$ ) the electronic charge, and  $K_B$  the Boltzmann constant.

The diffusion of oxygen vacancies occurs through the lattice defects and thereby called structure oxygen vacancies. In the samples of the present study, Zn ions occupy tetrahedral sites and Ni ions are present at octahedral sites, which leads to the migration of ferric ion from their original positions and the formation a lattice defect.

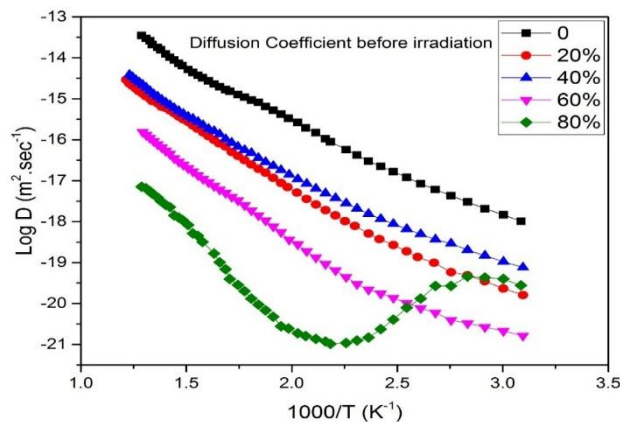


Fig. (3-a): Log D versus  $10^3/T$  before irradiated for the samples

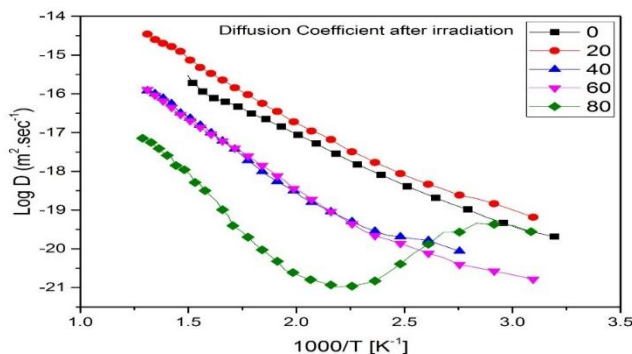


Fig. (3-b): Log D versus  $10^3/T$  after irradiated for the samples

Figure (4) presents the variation of diffusion coefficient of oxygen vacancies as a function of  $BaTiO_3$  content before and after irradiation. It is clear that the addition of  $BaTiO_3$  as a ferroelectric material decreases the diffusion coefficient due to the superstition of the diffusion of oxygen

vacancies through the lattice defect and the occupation of some lattice positions.

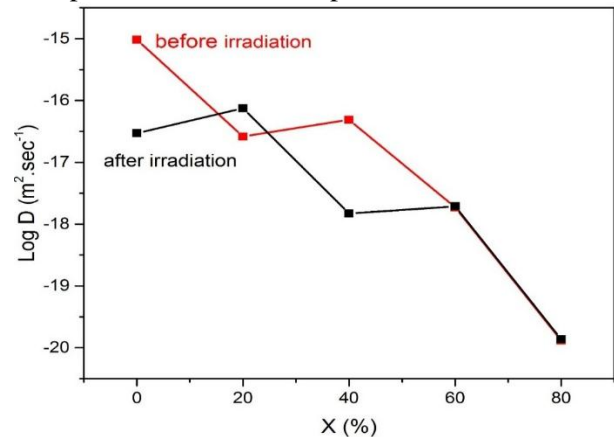


Fig. (4): Log D versus  $BaTiO_3$  content at room temperature before and after irradiation

As we know that the substitution of Zn ions instead of ferric ions at octahedral sites creates lattice vacancies, since the vacancy of  $Zn^{2+}$  ions is less than that of ferric ions vacancy.

The diffusion coefficient after irradiation decreases except for the sample 20%, this could be explained on the basis that the interaction of ionized  $\gamma$ -radiation with material generates more lattice vacancies which permits the displacement of ions from their equilibrium position and occupy the lattice vacancies. This process reduces the concentration of oxygen vacancies [12]

The activation energy for diffusion process before and after irradiation was calculated and given in Table (2). The diffusion activation energy is the sum of the oxygen atom migration energy ( $E_m$ ) and the vacancy formation energy ( $E_f$ );  $E = E_m + E_f$ . Moreover,  $E_f$  usually exceeds 1 eV which gives the evidence that the diffusion of oxygen in the given samples occurs through structural vacancies formation energy. [13].

The concentration of structural vacancies ( $n_v$ ) was calculated from the following expression [14]:

$$n_v = \frac{D_0}{a^2 v}$$

The concentration of structural vacancies increases after irradiation which confirms earlier discussion that the diffusion process increases after irradiation. The values of ( $n_v$ ) before and after irradiation are given in Table (2). This is considered an important attempt to calculate the concentration of structural vacancies in the material which can hardly be measured by any other technique.

**Table (2): The measured values of activation energy of diffusion process and the concentration of structural vacancies for unirradiated and irradiated sample samples**

Content %		0	20	40	60	80
After irradiation	Ef	0.181	0.169	0.150	0.139	0.346
Before irradiation	Ef	0.187	0.194	0.165	0.144	0.385
After irradiation	nv	4.35*10 <sup>-2</sup>	1.52*10 <sup>-1</sup>	3.23*10 <sup>-2</sup>	4.37*10 <sup>-2</sup>	1.04*10 <sup>-2</sup>
Before irradiation	nv	4.02*10 <sup>-1</sup>	1.68*10 <sup>-1</sup>	1.91*10 <sup>-1</sup>	4.09*10 <sup>-2</sup>	9.32*10 <sup>-3</sup>

### Magnetic permeability

The permeability as a function of temperature (300- 600 K) for all composite samples (BT-NZF) before and after irradiation are shown in Fig. (5a, 5b) respectively. The permeability was measured using a setup which is given in the previous work [15]. For samples zero and 20 % BT content, the permeability has a Hopkinson peak at low temperature associated with a sharp decrease in permeability reaching zero. The Curie Temperature  $T_c$  was determined by drawing a tangent for the linear part of permeability temperature curve as shown in Table (3), which increases by increasing BT content and after irradiation with  $\gamma$ -ray. As the BT content increases greater than 20 %, the behavior of the permeability changes which indicates that the BT became the predominant phase. According to Globus equation [16], the initial magnetic permeability is given by:

$$\mu_i = \frac{M_s T_m}{\sqrt{K_1}}$$

Where  $T_m$  is the average grain size,  $K_1$  is the magnetic crystalline anisotropic constant and  $M_s$  is saturation magnetization. Both  $K_1$  and  $M_s$  are temperature dependent factors.

The permeability of ferrite phase depends on the domain wall motion, which is greatly enhanced by the grain size. The greater are domain walls, the higher is the initial permeability. It was found that the values of permeability decrease after irradiation which is related to the decrease of grain size which was observed from the SEM micrograph as shown in Fig. (6c, 6d). Considering the magnetic anisotropic is constant, there is a direct proportionality between magnetic permeability and grain size. The decrease in the grain size affects the grain wall motion, which inhibits the value of the magnetic permeability after irradiation.

The SEM micrograph in Fig. (6) of nanocomposite samples shows the presence of two phases (tetragonal structure for ferroelectric phase and

cubic structure belongs to ferrimagnetic phase). The micrographs show a good densification and homogenous grain size with low porosity. Under the effect of  $\gamma$ - radiation which creates vacancies (defects) due to the agglomeration of domain walls and diffusion of ferrimagnetic phase and surrounding ferroelectric phase which leads to a decrease of the grain size as shown in Table (4). Another reason for the decrease of the grain size is the fracture of grains under the effect of irradiation leading to decrease of grain size [17, 18].

### Conclusion

For the ferromagnetic phase, the lattice constant before irradiation does not change remarkably with increase in the BT content  $g$ , but it slightly changes for the tetragonal phase (the lattice constant  $c$ ) decrease whereas  $a$  increase). By reassigning the temperature, the composite undergoes a change in conduction from semiconductor mechanism at low temperature to hopping conduction mechanism at a higher temperature. The change in DC resistivity occurs after irradiation and the Curie temperature (TC) decreases. For higher values of BT content, the TC increases due to the increase of the particle size after irradiation. It could be concluded that the diffusion coefficient after irradiation decreases except for the sample 20 %, this could be explained on the basis that the interaction of the ionized  $\gamma$ - radiation with material generates more lattice vacancies which permit the displacement of ions from their equilibrium position and occupy the lattice vacancies. This process reduces the concentration of oxygen vacancies. The activation energy for diffusion process decreases after irradiation. The permeability of ferrite phase depends on the domain wall motion, which is greatly enhanced by the grain size. The greater domain walls are the higher is initial permeability. It is found that the values of permeability decrease after irradiation which is related to the decrease of grain size which is observed from the SEM micrograph

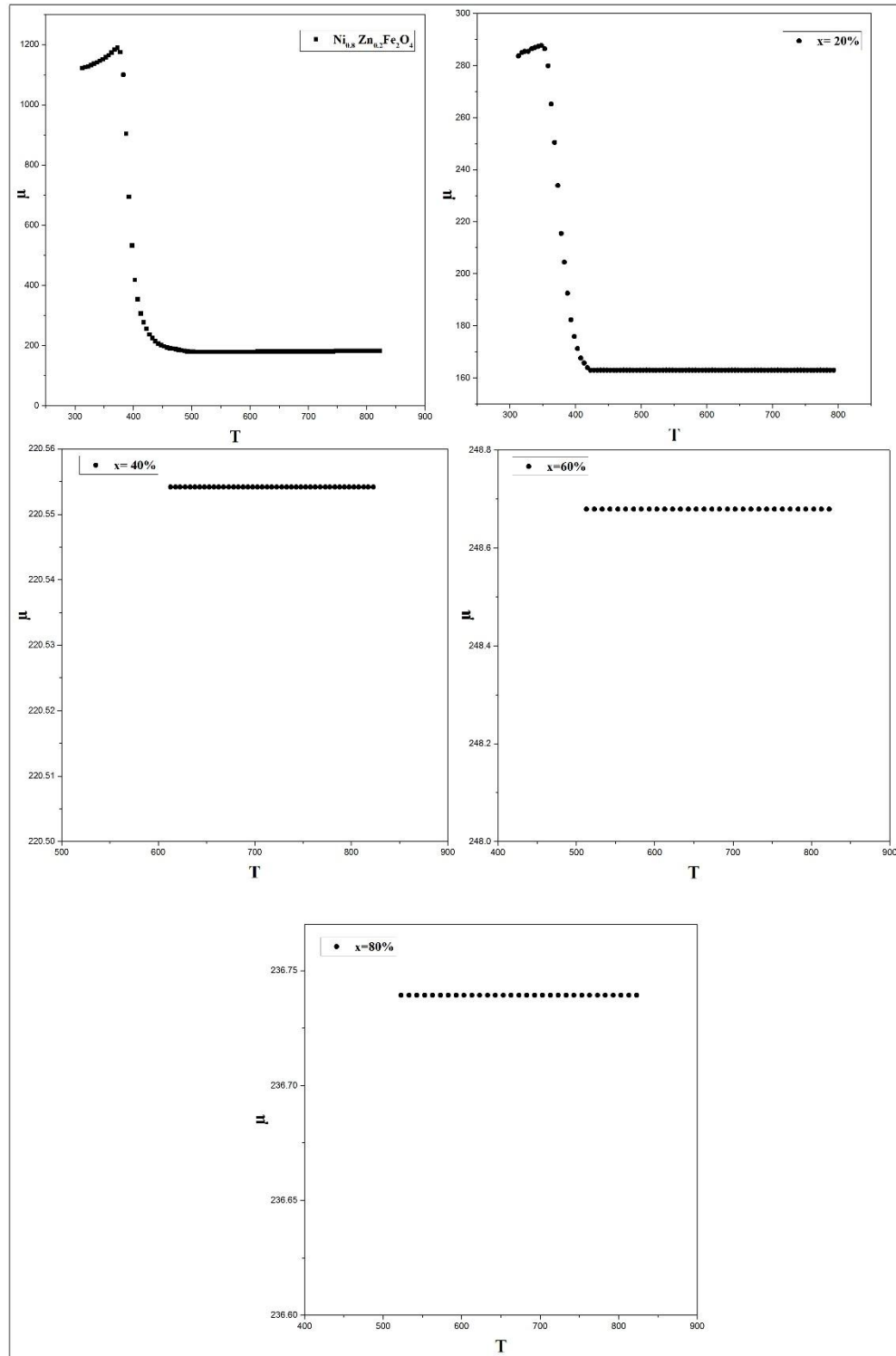


Fig. (5-a): Variation of initial permeability  $\mu_i$  with temperature of the composite  $(1-x)\text{Ni}_{0.8}\text{Zn}_{0.2}\text{Fe}_2\text{O}_4 + x\text{BaTiO}_3$  as a function of reciprocal temperature before irradiated with gamma ray

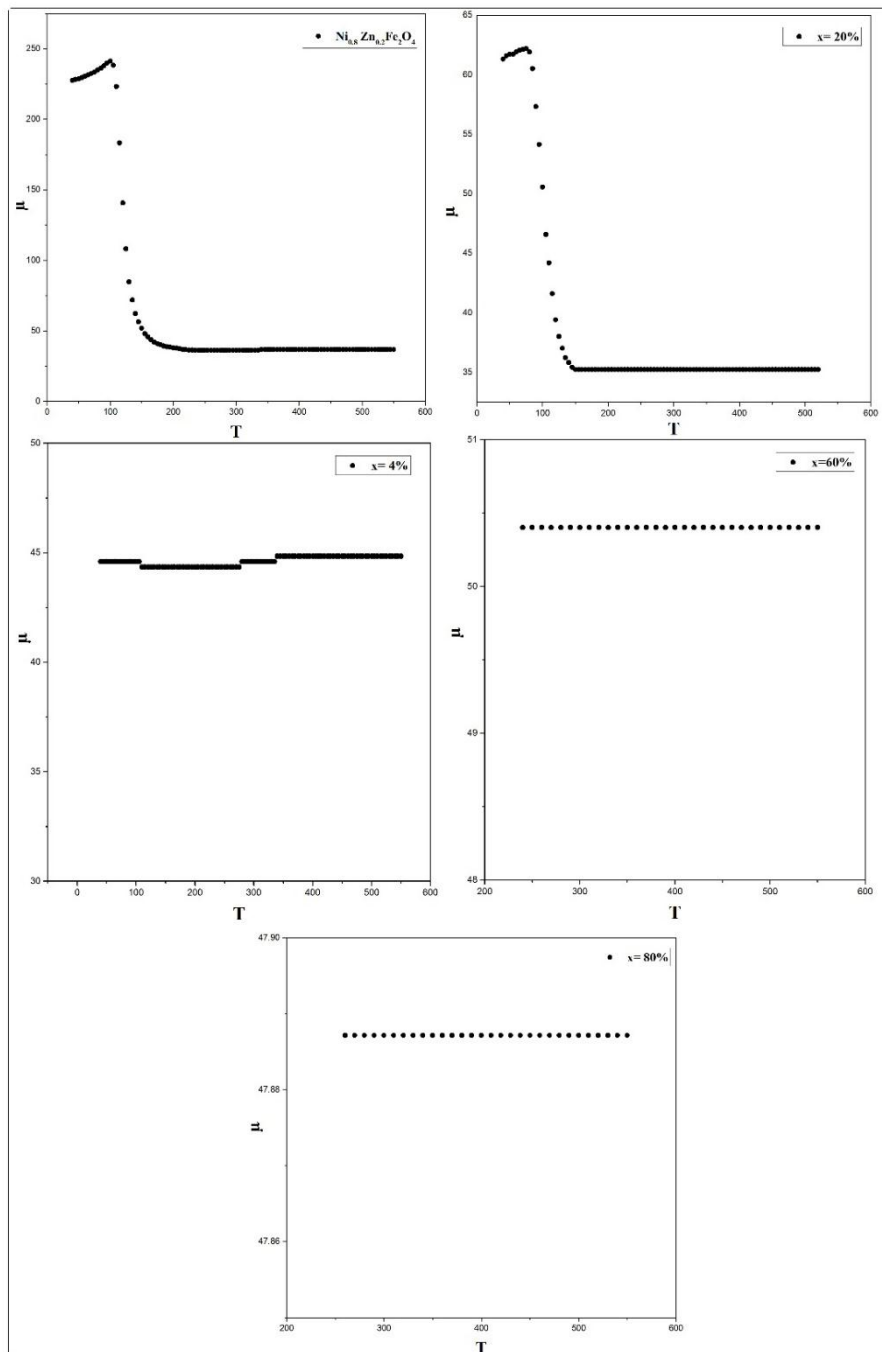
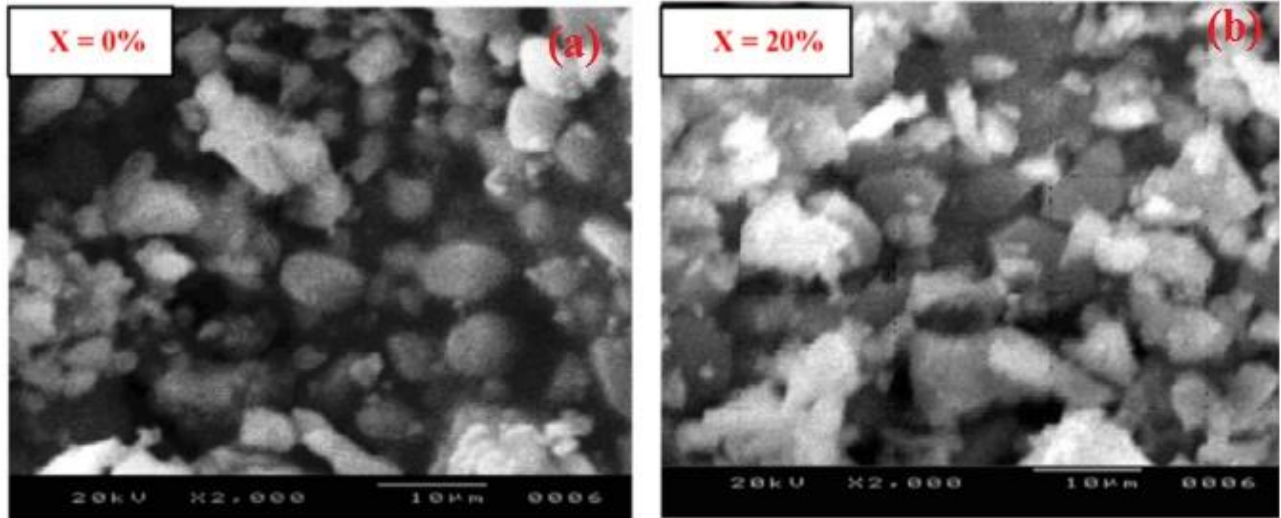
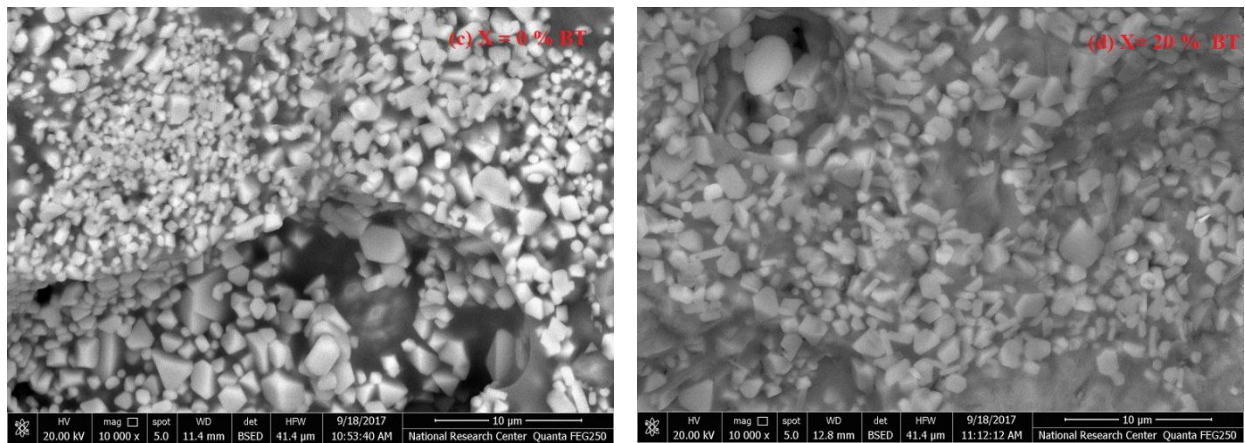


Fig. (5-b): Variation of initial permeability  $\mu_i$  with temperature of the composite  $(1-x) \text{Ni}_{0.8}\text{Zn}_{0.2}\text{Fe}_2\text{O}_4 + x \text{BaTiO}_3$  as a function of reciprocal temperature after irradiated with gamma ray

**Table (3): The measured values of curie temperature for unirradiated (D0) and irradiated sample (D1) samples**

Parameter	X=0		X=20	
	D <sub>0</sub>	D <sub>1</sub>	D <sub>0</sub>	D <sub>1</sub>
Curie temperature, T <sub>c</sub> (K) from permeability.	310	393	420	423

**Fig. (6a, 6b): The SEM micrograph for the composite samples (1-X) Ni<sub>0.8</sub>Zn<sub>0.2</sub>Fe<sub>2</sub>O<sub>4</sub>+ (x) BaTiO<sub>3</sub> before irradiated with gamma ray****Fig. (6c, cd): The SEM micrograph for the composite samples (1-X) Ni<sub>0.8</sub>Zn<sub>0.2</sub>Fe<sub>2</sub>O<sub>4</sub>+ (x) BaTiO<sub>3</sub> after irradiated with gamma ray**

**Table (4): The grain size of (1-X) Ni<sub>0.8</sub>Zn<sub>0.2</sub>Fe<sub>2</sub>O<sub>4</sub>+ (x) BaTiO<sub>3</sub> for unirradiated (D0) and irradiated sample (D1) samples**

Composition	100% Ni <sub>0.8</sub> Zn <sub>0.2</sub> Fe <sub>2</sub> O <sub>4</sub>		20% BaTiO <sub>3</sub> + 80% Ni <sub>0.8</sub> Zn <sub>0.2</sub> Fe <sub>2</sub> O <sub>4</sub>	
	Grain Size, (μm)			
	D <sub>0</sub>	D <sub>1</sub>	D <sub>0</sub>	D <sub>1</sub>
<b>Ferrimagnetic phase</b>	3.34	0.430	2.96	0.777
<b>Ferroelectric phase</b>	---	---	1.38	0.370

### References

- J.H. Shen, Y. Bai, J. Zhou and L.T. Li, Journal of the American Ceramic Society. 88 (2005) 3440-3443.
- H. Zheng, et al., Philosophical Transactions of the Royal Society A. 13 (2011) 3069-3097.
- A. Tawfik, O.M. Hemed, A.M.A. Henaish and A.M. Dorgham, Journal of Materials Chemistry and Physics. 211 (2018) 1-8.
- W. Qiu, H.H. Hng, Effects of dopants on the microstructure and properties of PZT ceramics, Mater. Chem. Phys. 75 (1) (2002) 151 - 156.
- O.M. Hemed, et al., Journal of Magnetism and Magnetic Materials. 324 (2012) 4118-4126.
- M. Takatw, D. Tsubone and H. Yanagida, Phy. Abstract. 78 (1975) 1009.
- A. Lakshman, P.S. Sobbarao and K.H. Rao. Journal of Magnetism and Magnetic Materials. 283 (2004) 326-334.
- H.E. Hassan, et al., Nuclear Instruments and Methods in Physics Research B.304 (2013) 72-79.
- N. Okasha, J. Alloys Compd. 490 (2010) 307-310.
- P. Mishra, P. Kumar, Adv. Condens. Matter Phys. 2013 (2013) 858406, 9.
- O.M. Hemed, et al., Journal of Magnetism and Magnetic Materials.390 (2015) 70-77.
- O.M. Hemed, M. El-Saadaw, Journal of Magnetism and Magnetic Materials.256 (2003) 63-68.
- H. S, Marek and H. B. Serreze, Applied Physics Letters.51 (1987) 2031-2033.
- E.E. Maller, A. Akerstvom, Z. Phys. Chem. (Leipzig).1067 (1997) 163.
- O.M. Hemed, Journal of Magnetism and Magnetic Mater 251 (2002) 60-69.
- A. Globus, P. Duplex, M. Cryot, IEEE Transactions on Magnetics 7-3 (1971)617-622.
- U. Ahmadu, et al., Processing and Application of Ceramics .10 [2] (2016) 79-85.
- A. K. Nath and A. Medhi, Indian J. phys. 89 [2] (2015) 131-136.